Journal of Catalysis 256 (2008) 259–267

Contents lists available at ScienceDirect

Journal of Catalysis

www.elsevier.com/locate/jcat

High-activity, single-site mesoporous WO_3-MCF materials for the catalytic epoxidation of cycloocta-1,5-diene with aqueous hydrogen peroxide

Ruihua Gao [a], Xinli Yang [a,b], Wei-Lin Dai [a,*], Yingyi Le [a], Hexing Li [c], Kangnian Fan [a]

[a] Department of Chemistry and Shanghai Key Laboratory of Molecular Catalysis and Innovative Materials, Fudan University, Shanghai 200433, PR China
[b] School of Chemistry and Chemical Engineering, Henan University of Technology, Henan 450052, PR China
[c] Department of Chemistry, Shanghai Normal University, Shanghai 200234, PR China

ARTICLE INFO

Article history:
Received 4 December 2007
Revised 20 March 2008
Accepted 20 March 2008
Available online 24 April 2008

Keywords:
Isolated tetrahedral {WO_4} species
Mesocellular silica foam (MCF) catalyst
Epoxidation
Cycloocta-1,5-diene

ABSTRACT

For the first time, the high-activity, single-site mesoporous WO_3-MCF materials were synthesized and characterized by N_2 sorption, TEM, UV–vis DRS, UV-Raman, and XPS. It was found that the dispersion and nature of the tungsten species depend strongly on the tungsten oxide content and the support characteristic. The novel catalyst remains a highly ordered mesostructure of the silica support. The catalytic performance of the materials in the epoxidation of cycloocta-1,5-diene with aqueous H_2O_2 was investigated. The excellent catalytic performance of WO_3-MCF in the selective oxidation of cycloocta-1,5-diene was attributed to the presence of isolated tetrahedral {WO_4} species and the unique pore structure. The novel catalyst can be easily recycled after reaction and reused many times with no significant loss of activity. The good stability can be attributed to the presence of isolated tungsten species anchored on the support through W–O–Si covalent bonds.

1. Introduction

Tungsten-containing materials have been widely used in the metathesis and isomerization of alkenes [1], selective oxidation of unsaturated compounds [2], dehydrogenation of alcohols [3], and hydrodesulfurization and hydrocracking of heavy fractions in petroleum chemistry [4,5]. In addition, many research groups have attempted to synthesize mesoporous tungsten oxide materials [6] or to incorporate tungsten into nonsiliceous mesostructured materials, including TiO_2 [7,8] and siliceous mesoporous molecular sieves (e.g., silica, M41S, SBA-n) by impregnation [9], cogelation [10], insertion [11–14], or grafting [15]. But the structure of the nonsupported tungsten oxide mesoporous materials is not thermally stable and will collapse on high-temperature calcination. Meanwhile, tungsten-containing mesoporous molecular sieves also have some serious drawbacks, including (1) difficult-to-control dispersion of the tungsten species, allowing the preferential formation of tiny tungsten oxide particles even at relatively low concentrations; (2) structural collapse of the mesoporous materials after high-temperature calcinations and/or after a certain amount of metal loading; and (3) an inherent leaching problem, which causes confusion as to the heterogeneity of the catalysts. To minimize this leaching problem, much effort has been focused on synthesizing materials in which the active tungsten species are well isolated and anchored on the support through W–O–Si covalent bonds.

It is commonly accepted that the catalytic behavior of the supported tungsten oxides is sensitive to the intrinsic nature of the tungsten species, including oxidation state, coordination circumstance, dispersion, and stability. On the other hand, the chemical and structural features of the supports affect catalytic performance either indirectly, by influencing tungsten dispersion and stabilization of the tungsten oxide species, or directly, by forming a shape-selective catalyst. Therefore, it is very important to study the effect of the supports and the relationship between the catalytic performance of the catalysts and the tungsten oxidation state, coordination circumstance, dispersion and stability.

There are some other oxidation catalysts with isolated active sites. The dispersion and the nature of the vanadium oxide species also affect the catalytic behavior of VO_x-based catalysts. Berndt et al. [16] reported that isolated vanadium oxide species are active sites for the partial oxidation of methane. They also reported that vanadium species catalyzes the oxidative dehydrogenation of propane in both valence states, V^{5+} and V^{4+}; however, V^{4+} seems to be more selective, although less active, than V^{5+}, due to its lower oxidation potential [17]. Fe-ZSM-5 zeolites are recognized as highly efficient catalysts for numerous reactions; however, debate on the nature of the active Fe sites in these catalysts is ongoing [18,19]. This is due mainly to the fact that in most cases, depending on the preparation method and the Fe content, various coexisting Fe species are created, ranging from isolated Fe ions via dimers and small oligonuclear Fe_xO_y clusters inside the pores to large Fe_2O_3

* Corresponding author. Fax: +86 21 65642978.
E-mail address: wldai@fudan.edu.cn (W.-L. Dai).

0021-9517/$ – see front matter
doi:10.1016/j.jcat.2008.03.017

particles on the external surface. According to Santhosh Kumar et al. [20], for both NH_3 and *i*-butane-SCR (selective reduction of NO), the concentration of accessible Fe^{3+} that can participate in a reversible redox cycle should be maximized, whereas the formation of Fe_xO_y clusters must be completely (for *i*-butane-SCR) or largely (for NH_3-SCR) avoided, indicating that Fe^{3+} may play a major role in the catalytic cycle.

In recent years, there has been considerable interest in the catalytic epoxidation of alkenes, which is an efficient and accessible approach to the intermediates and precursors of many useful chemical products. Epoxidation of cycloocta-1,5-diene (COD) has been investigated using several metal catalysts under both homogeneous [21–24] and heterogeneous [25] conditions. Pillai et al. [26] prepared effective catalyst systems for COD epoxidation using hydrogen peroxide. Although these systems offer good catalytic activity in the epoxidation of COD, their use of acetonitrile is a significant limitation. In previous work [27], we found that WO_3-containing mesocellular silica foam (MCF) catalysts showed high activity in the *O*-heterocyclization of COD, but that detectable leaching of tungsten species from 10%WO_3-MCF occurred, according to ICP-AES analysis. It is known that leaching of tungsten species is inevitable in most reactions with H_2O_2; therefore, there is a strong impetus to find a more stable catalyst with no leaching of tungsten species, to avoid the generation of heavy metal-containing wastewater. In previous studies, we identified several tungsten species on the catalyst surface, including isolated tetrahedral {WO_4} species, low-condensed polymeric tungsten oxide species, high-condensed polymeric tungsten oxide species, and small particles of crystalline WO_3; however, which of these is the most important for the oxidation with H_2O_2 remains unclear. Based on the widely accepted concept that the isolated tetrahedral {WO_4} species must be the most simple and stable in most reactions, we have designed a novel isolated tetrahedral {WO_4} species containing WO_3-MCF catalyst.

In the present work, to gain insight into the key role of isolated tetrahedral {WO_4} species on MCF materials in the catalytic oxidation of COD with H_2O_2, we synthesized the isolated tetrahedral {WO_4} species-doped MCF materials via different methods and systematically characterized these materials by various analytical and spectroscopic techniques, including N_2 sorption, TEM, UV–vis DRS, UV-Raman, and XPS.

2. Experimental

2.1. Catalyst preparation

In a typical procedure for the synthesis of WO_3-MCF catalyst [27], first 4.5 g of Pluronic P123 triblock polymer ($EO_{20}PO_{70}EO_{20}$, $M_{av} = 5800$, Aldrich) was added to 170 mL of 1.6 M HCl and stirred for 4 h at 40 °C, and then 4.5 g of 1,3,5-trimethybenzene (TMB) was added to the solution and stirred for 2 h. After that, 9.9 g of $Si(OC_2H_5)_4$ (TEOS) was added to the mixture; after stirring for another 15–20 min, 6.2 mL of sodium tungstate ($Na_2WO_4{\cdot}2H_2O$, 0.2 M) aqueous solution was added. The resulting mixture was then aged at 40 °C under moderate stirring for 24 h and crystallized at 100 °C for another 24 h. The resulting solid product was filtered, washed with distilled water, dried at room temperature, and then calcined at 500 °C in air for 8 h to remove the template. The resulting material, designated WO_3-MCF-as-syn, was finally treated with 1 M of ammonium acetate (AMA) at 80 °C for 6 h (designated 10%WO_3-MCF-1) [28]. Under such conditions, the tungsten percentage in the solution and in the catalyst rapidly achieved a balance when the catalyst was treated with AMA. A sample treated twice is designated 10%WO_3-MCF-2; one treated three times is designated 10%WO_3-MCF-3. The 20%WO_3-MCF and 30%WO_3-MCF were synthesized by the same method, only with different volumes of sodium tungstate ($Na_2WO_4{\cdot}2H_2O$, 0.2 M) aqueous solution. Here 10, 20, and 30% represent the theoretical weight ratio of WO_3 to silica over the materials before treatment with AMA. ICP analysis indicated an Si/W molar ratio of 942 for 10%WO_3-MCF-1 after AMA treatment (compared with 55 before AMA treatment), suggesting that more than 94% of the loosely bonded tungsten species were removed by AMA solution.

In a typical procedure for the synthesis of 10%WO_3-SBA-15-1 catalyst, first 5 g of Pluronic P123 triblock polymer ($EO_{20}PO_{70}EO_{20}$, $M_{av} = 5800$, Aldrich) and 28 g of distilled water were added to 150 mL of 2 M HCl and stirred for 4 h at 40 °C. After 10 g of TEOS was added and the mixture was stirred for another 30 min, 6.2 mL of an aqueous solution of sodium tungstate ($Na_2WO_4{\cdot}2H_2O$, 0.2 M) was added. The resulting mixture was aged at 40 °C under moderate stirring for 24 h, and then crystallized at 95 °C for 3 days. The solid product was filtered, washed with distilled water, and then dried at room temperature. After calcination at 500 °C in air for 5 h to remove the template, the product was treated with 1 M AMA at 80 °C for 6 h (designated 10%WO_3-SBA-15-1) [28].

The impregnation method-derived 10%WO_3/MCF-1, 10%WO_3/SBA-15-1, and 10%WO_3/MCM-41-1 catalysts were synthesized as follows. The prespecified amount of ammonium tungstate was dissolved in an aqueous solution of ammonia. The MCF materials (prepared following a procedure similar to that reported by Schmidt-Winkel et al. [29]), SBA-15 [30,31], and MCM-41 [32], were added into the stirred solution at 60 °C. Then the excessive water was completely evaporated at the same temperature, and the catalyst was finally obtained after calcination at 550 °C in air for 3 h and then treated with 1 M AMA at 80 °C for 6 h (designated 10%WO_3/MCF-1, 10%WO_3/SBA-15-1, and 10%WO_3/MCM-41-1) [28].

2.2. Characterization

The specific surface area, pore volume, and the pore size distribution (PSD) of the samples were measured and calculated according to the BET method on a Micromeritics TriStar 3000 analyzer with liquid nitrogen at −196 °C. The BJH method was used to determine PSD. Transmission electron microscopy (TEM) images were obtained with a Joel JEM 2010 microscope.

The UV-Raman measurements were carried out on a confocal microprobe Jobin Yvon LabRam Infinity Raman system using the UV line at 325 nm from a Kimmon IK3201R-F He-Cd laser as the exciting source. The laser output was 30 mW, and the maximum incident power at the sample was approximately 6 mW. UV–vis DRS spectra were collected on a Shimadzu UV-2540 spectrometer with $BaSO_4$ as a reference.

The XPS spectra were recorded on a Perkin–Elmer PHI 5000C ESCA system equipped with a dual X-ray source, using the Mg$K\alpha$ (1253.6 eV) anode and a hemispherical energy analyzer. The background pressure during data acquisition was kept below 10^{-6} Pa. Measurements were performed at pass energy of 93.90 eV to ensure sufficient sensitivity for the acquisition scan; a pass energy of 23.50 eV was used for the scanning of the narrow spectra of Si2p, W4f, O1s, and C1s to ensure sufficient resolution. All binding energies were calibrated using contaminant carbon (C1s = 284.6 eV) as a reference.

The tungsten content was determined by inductively coupled argon plasma analysis (ICP; IRIS Intrepid, Thermo Elemental Company) after the samples were solubilized in an HF:HCl solution.

2.3. Activity test

The activity test was performed at 60 °C with magnetic stirring in a closed 25-mL regular glass reactor using 50% aqueous H_2O_2 as the oxygen donor and *t*-BuOH as the solvent. In a typical experiment, 0.53 mL of COD (3.6 mmol), 10 mL of *t*-BuOH, and

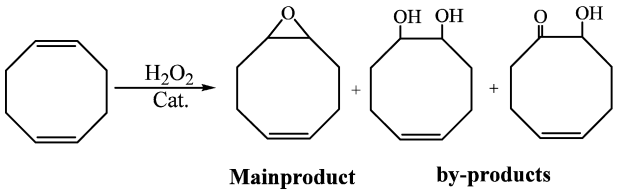

Scheme 1. Main-product and byproducts from the epoxidation of cycloocta-1,5-diene by aqueous H_2O_2.

0.2 g of the WO_3-MCF-1 material (10%) were introduced into the regular glass reactor at 60 °C and stirred vigorously. The reaction was initiated by the addition of 0.7 mL of 50 wt% aqueous H_2O_2 (11.3 mmol) into the mixture, which was held for 24 h. The main product (designated MD) and byproducts from the epoxidation of COD by aqueous H_2O_2 are listed in Scheme 1. Quantitative analysis of the reaction products was performed by gas chromatography (GC) and the identification of different products in the reaction mixture was determined by GC-mass spectrometry (GC-MS) on an HP 6890GC/5973 mass spectrometer.

3. Results and discussion

3.1. Catalyst characterization

3.1.1. Pore size distribution from nitrogen adsorption

Fig. 1 shows that the nitrogen adsorption/desorption isotherms of 10%WO_3-MCF-1 and 10%WO_3/MCF-1 were of type IV and exhibited steep hysteresis of type H1 at high relative pressures. The pore size distribution of these two samples unambiguously demonstrates preservation of the 3-D mesocellular structure of the support. Meanwhile, the nitrogen isotherms of 10%WO_3-SBA-15-1 and 10%WO_3/SBA-15-1 also were type IV, and the pore size distribution of these two samples clearly indicated retention of the typical 2-D pore structure of SBA-15. The 10%WO_3/MCM-41-1 also exhibited reversible hysteresis-free type IV isotherms, and the pore size distribution clearly showed the 2-D pore structure of MCM-41. The pore size of these samples had the following hierarchy: 10%WO_3-MCF-1 ∼ 10%WO_3-MCF-1 > 10%WO_3-SBA-15-1 ∼ 10%WO_3/SBA-15-1 > 10%WO_3/MCM-41-1.

3.1.2. Surface morphology from TEM measurements

TEM images (Fig. 2) of 10%WO_3-MCF-1 (Fig. 2a) and 10%WO_3/MCF-1 (Fig. 2b) materials reveal a disordered array of silica struts composed of uniform-sized spherical cells (18–24 nm) interconnected by windows with a narrow size distribution. This is a characteristic structural feature of the MCF materials [29,33].

3.1.3. Isolated sites by UV–vis DRS

The DRS spectra obtained in the UV–vis region of the as-synthesized WO_3-containing MCF samples shown in Fig. 3a provide information on the chemical nature and coordination states of tungsten oxide species. This technique is known to be highly sensitive in distinguishing incorporated metal oxide and extra-framework metal oxides in different mesostructures [34]. For comparison, the figure also shows UV–vis DRS spectra of sodium tungstate ($Na_2WO_4{\cdot}2H_2O$) and bulk WO_3. The spectrum of sodium tungstate, with a spinel structure and isolated $[WO_4]^{2-}$ tetrahedral species, is characterized by a maximum at 230 nm (curve a) [35]. For pure mesocellular silica MCF, no bands are evident in the spectrum. After introduction of tungsten oxide into MCF, three Raman bands appeared at 230, 290, and 430 nm. The broad band at about 430 nm of the 30 wt% WO_3-MCF-as-syn. and 20 wt% WO_3/MCF-as-syn. samples can be attributed to tungsten trioxide by comparing it with the spectrum of bulk WO_3 [36]. The second broad band at about 290 nm represents another kind of tungsten oxide species.

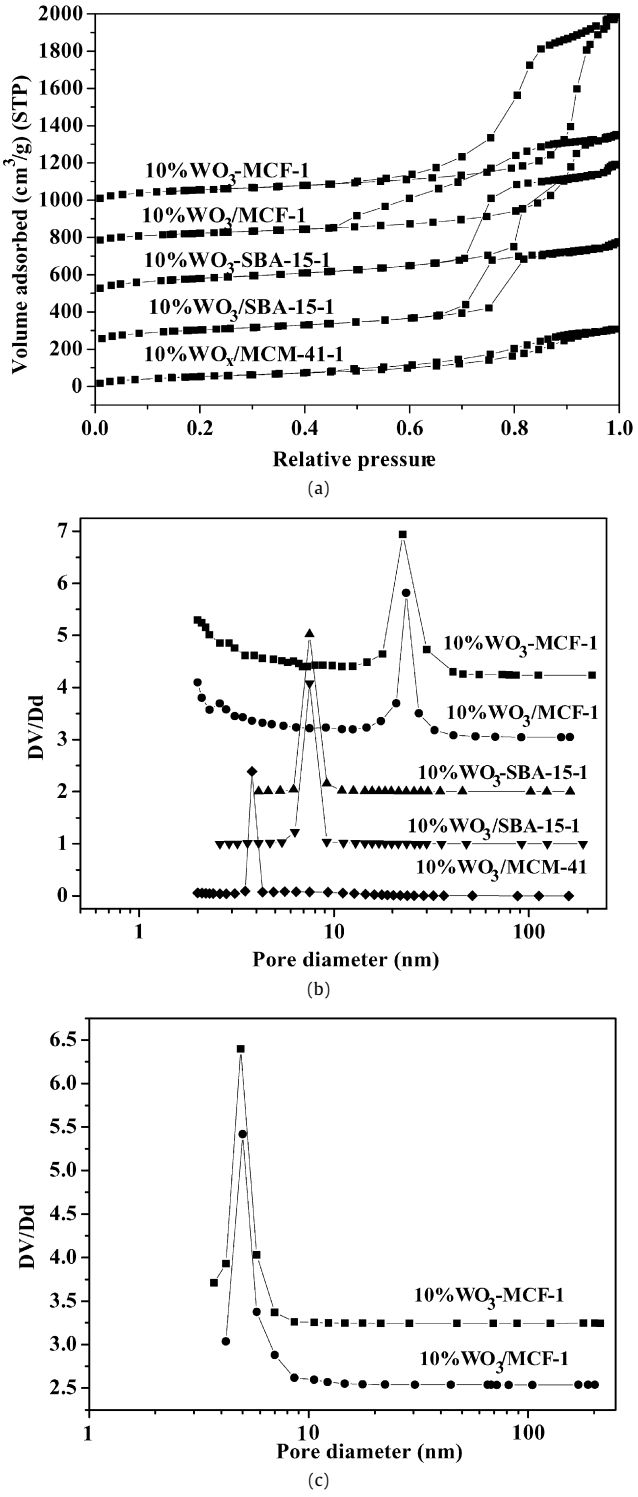

Fig. 1. Nitrogen adsorption–desorption isotherms for the novel materials (a); pore size distribution for various samples based on a BJH method, desorption branches for pore distribution (b); adsorption branches for window distribution (c). The ratio of WO_x to silica over all materials was 10%.

Weber et al. reported that the low-energy absorption edge shifted toward a lower wavelength with decreasing nuclearity of molybdenum and tungsten entities [37]; therefore, this broad band should be assigned to isolated tungsten species or low-condensed polymeric tungsten oxide species. The sharp band at 230 nm of the *in situ* synthesized sample can be attributed to isolated $[WO_4]^{2-}$ tetrahedral species by comparing it with the structure of sodium

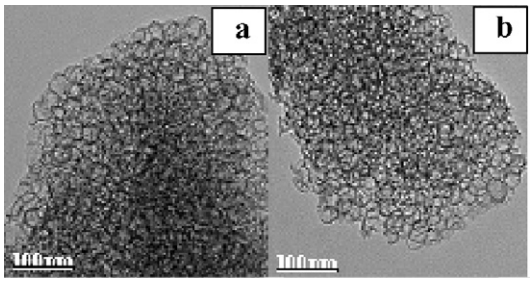

Fig. 2. TEM images of different WO_3-MCF materials: 10%WO_3-MCF-1 (a) and 10%WO_3/MCF-1 (b).

tungstate. The absence of a broad band at 430 nm may reflect the high dispersion of tungsten oxide species and lack of crystalline WO_3 formation in WO_3-containing MCF samples with tungsten oxide content <20 wt%. A weak band at 430 nm for the 20 wt% WO_3-MCF sample indicates the formation of only a small amount of low crystalline WO_3 species. Further increases in the tungsten oxide content up to 30 wt% will lead to the formation of a large quantity of crystalline WO_3 species, resulting in the appearance of a strong band at 430 nm. The UV–vis DRS spectra further demonstrate that the chemical nature and coordination states of tungsten oxide species are determined by the WO_3 loadings.

The DRS spectra recorded in the UV–vis region of the AMA-treated WO_3-containing MCF samples given in Fig. 3b show significant differences between the spectra of the AMA-treated samples and the as-synthesized samples. The 10%WO_3-MCF-1 sample exhibited only one band at 230 nm, attributed to isolated $[WO_4]^{2-}$ tetrahedral species. For the 20%WO_3-MCF-1, two Raman bands appeared at 230 and 290 nm and the weak band at 430 nm disappeared, indicating removal of a small amount of low-crystalline WO_3 species. For the 30%WO_3-MCF-1, the band at 430 nm was much less intense than that for the as-synthesized sample, indicating removal of most crystalline WO_3 species by the AMA treatment. Similar investigations by UV–vis spectroscopy reported by Berndt et al. [16] showed that the vanadium species on 2.8V/MCM-41 were monomeric and oligomeric tetrahedrally coordinated V^V species, as well as square pyramidal and distorted octahedral V^V species. After the sample was heated in flowing nitrogen to 823 K, only monomeric and oligomeric tetrahedrally coordinated V^V species remained.

DRS spectra recorded in the UV–vis region of the as-synthesized and AMA-treated 10%WO_3/MCF samples are shown in Fig. 3c. For the as-synthesized 10%WO_3/MCF, three Raman bands appeared at 230, 290, and 430 nm; the very weak peak at 430 nm indicates the presence of high-condensed polymeric tungsten oxide species. Only two bands, at 230 and 290 nm, remained on the sample after one AMA treatment, indicating removal of the high-condensed polymeric tungsten oxide species. After two AMA treatments, the peak of 290 nm was much weaker, demonstrating removal of the low-condensed polymeric tungsten oxide species. After three AMA treatments, the two bands at 230 and 290 nm were similar to those of the 10%WO_3/MCF-2, indicating that the remaining tungsten oxide species were the isolated tetrahedral $[WO_4]^{2-}$ species anchored on the support through W–O–Si covalent bonds, which cannot be removed by AMA treatment.

3.1.4. Tungsten percent by ICP

Fig. 4 illustrates the dependence of the residual tungsten percent of the AMA-treated catalysts on the tungsten content of the as-synthesized WO_3-MCF catalysts. As shown, the residual tungsten percent increased rapidly initially and maintained a fixed value of 0.30 from the value at a tungsten loading of 3.94% for the as-synthesized catalyst. This finding indicates that the MCF has a fixed maximal value (0.30%) and that the tungsten can be

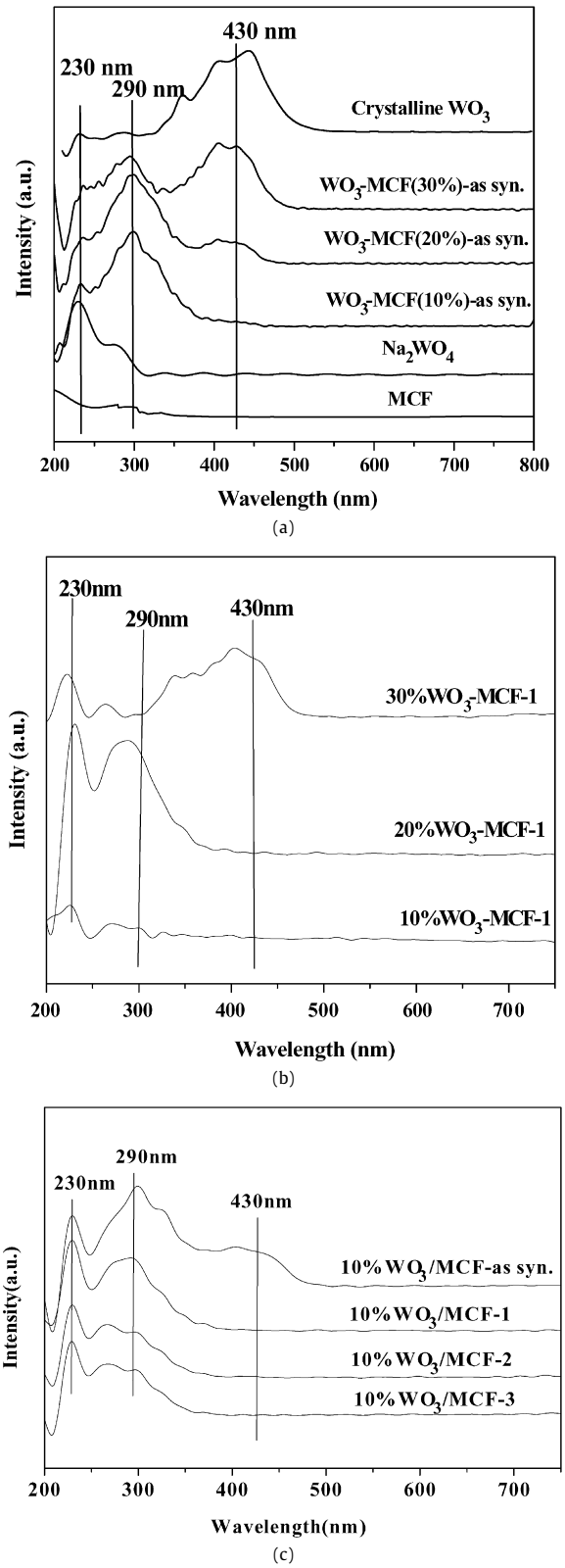

Fig. 3. Diffuse reflectance spectra in the UV–vis region of the as-synthesized WO_3-containing MCF samples (a); the AMA-treated WO_3-containing MCF samples (b); the as-synthesized and AMA-treated 10%WO_3/MCF samples (c).

incorporated very stably into the MCF framework. Based on this interesting result, we can conclude that for these novel catalysts, the residual tungsten species are the isolated tetrahedral $[WO_4]^{2-}$ species anchored on the support through W–O–Si covalent bonds. The loosely bonded tungsten species are completely removed by

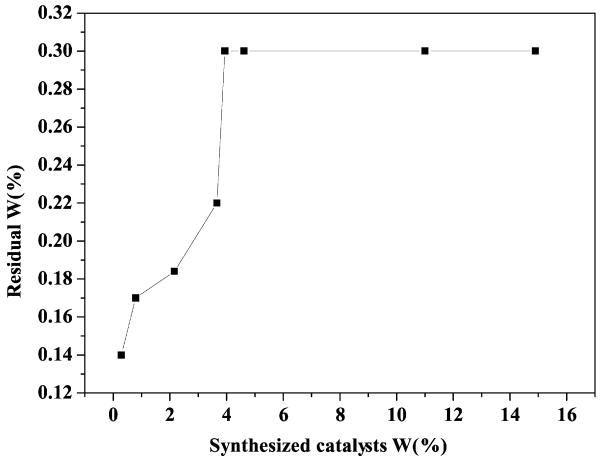

Fig. 4. Dependence of the residual tungsten percent of the AMA-treated catalysts on the tungsten content of the as-synthesized WO_3-MCF catalysts.

Table 1
ICP results of the different catalysts over the different supports

Catalyst	W (%)[b]	W (%)[a]	Si/W (mol)[b]	Si/W (mol)[a]
10%WO_3-MCF-1	0.30	4.61	941.7	54.5
10%WO_3/MCF-1	1.11	6.75	253	41.5
10%WO_3-SBA-1	0.29	4.02	975.9	65.4
10%WO_3/SBA-1	0.80	6.74	340.5	41.5
10%WO_3/MCM-1	1.20	6.77	244.2	41.4

[a] The as-synthesized value.
[b] The AMA-treated value.

Table 2
ICP results of the different catalysts over the different WO_3 loadings

Catalyst	W (%)[b]	W (%)[a]	Si/W (mol)[b]	Si/W (mol)[a]
10%WO_3-MCF-1	0.3	4.61	941.7	54.5
10%WO_3-MCF-2	0.3	0.3	943	941.7
20%WO_3-MCF-1	0.5	11.1	589.0	22.7
20%WO_3-MCF-2	0.3	0.5	1062	589.0
30%WO_3-MCF-1	1.7	14.9	179.0	14.2
30%WO_3-MCF-2	0.3	1.7	998	179.0

[a] The as-synthesized value.
[b] The AMA-treated value.

the AMA treatment. In addition, a tungsten loading of about 4% was sufficient to obtain an efficient single-site tungsten-containing catalyst, suggesting that further tungsten loading would lead only to loosely bounded tungsten species. Even if the 4% loading one, only 7.6% tungsten species were effective and contributed to the isolated and stable covalent bonded $\{WO_4\}$ species. This finding also demonstrates that most of the tungsten species in the tungsten-containing silica catalysts, even those prepared by the *in situ* method, were not very stable and could be readily eluted by the AMA treatment.

Table 1 shows that the tungsten percent was much lower in the AMA-treated catalyst than in the as-synthesized catalyst in all cases studied, and that the tungsten percent was lower in the AMA-treated catalysts synthesized by the *in situ* method than in those synthesized by impregnation. However, the similar tungsten percent in the 10%WO_3-MCF-1 and 10%WO_3-SBA-1 samples indicate that different silica supports had the same percentage of tungsten stably incorporated into the silica framework.

The ICP results for the catalysts with different WO_3 loadings, given in Table 2, demonstrate that the tungsten content of these catalysts differed after one AMA treatment but were similar after two AMA treatments. This finding suggests that for the *in situ* method, one AMA treatment could not remove all of the loosely bound tungsten species, and that higher tungsten loading led to a higher percentage of tungsten remaining on the catalyst, and also that no matter how much tungsten was added, the percent of tungsten incorporated into the MCF framework remained a fixed value, and two AMA treatments are sufficient to obtain the most stable single-site tungsten-containing catalyst.

Table 3
ICP results of the 10%WO_3/MCF over the different AMA-treated number

Catalyst	W (%)	Si (%)	Si/W (mol)
10%WO_3/MCF-1	1.1	42.9	253
10%WO_3/MCF-2	0.70	42.8	403
10%WO_3/MCF-3	0.72	41.6	390

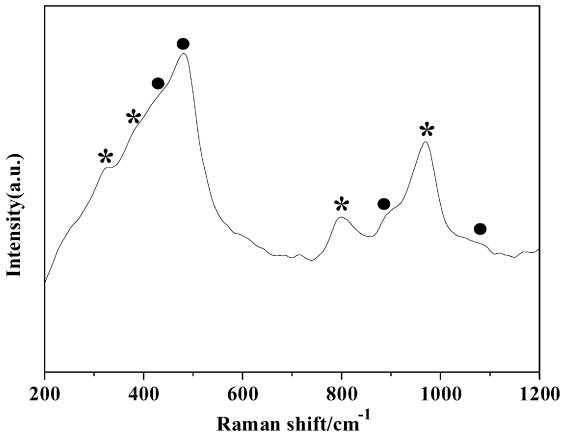

Fig. 5. UV-Raman spectra of the WMCF materials (*) represent the fundamental vibration of $\{WO_4\}$, the other modes (●) represent the fundamental vibration of silica.

The ICP results for the 10%WO_3/MCF catalyst after different AMA treatments, given in Table 3, show that the tungsten percentage remained constant after two AMA treatments. This indicates that the percent tungsten incorporated into the MCF framework remained fixed at a higher level in the impregnation-derived catalyst than the *in situ*-derived one. It is interesting to note that although over the impregnated catalyst more tungsten was incorporated into the silica framework, the selectivity in the COD selective oxidation was much lower, suggesting that the remaining tungsten species were not the same as single-site $\{WO_4\}$ tetrahedral even though they cannot be removed by two or more AMA treatments. This finding agrees well with the conclusions drawn from Tables 1 and 2 and our UV–vis DRS findings. Thus, we can conclude that the percentage of tungsten incorporated into the silica support is determined by the preparation method, and that only the *in situ* method can lead to the perfect single-site $\{WO_4\}$ tetrahedral.

3.1.5. Single sites by UV-Raman

The UV-Raman spectra shown in Fig. 5 provide further insight into the exact molecular structure of our AMA-treated WO_3-MCF materials. The bands at 320, 382, 800, and 970 cm^{-1} are assigned to the vibration of the isolated $\{WO_4\}$ structure [38], whereas those at 433, 480, 891, and 1078 cm^{-1} are associated with vibrations of the siloxane rings of MCF [39]. Clearly, the tungsten clusters on the surface are single-site $\{WO_4\}$ species bound strongly to silica through W–O–Si covalent bonds, as illustrated in Scheme 2. Similarly, Berndt et al. [16] detected V^{IV} species incorporated into the siliceous walls by ESR. The large amounts of loosely bonded tungsten species on the surface were readily removed on AMA treatment, and the oxotungsten tetrahedra centers into the framework maintained the structure of pure MCF. The UV-Raman results provide direct evidence of the presence of single-site tetrahedra $\{WO_4\}$ species.

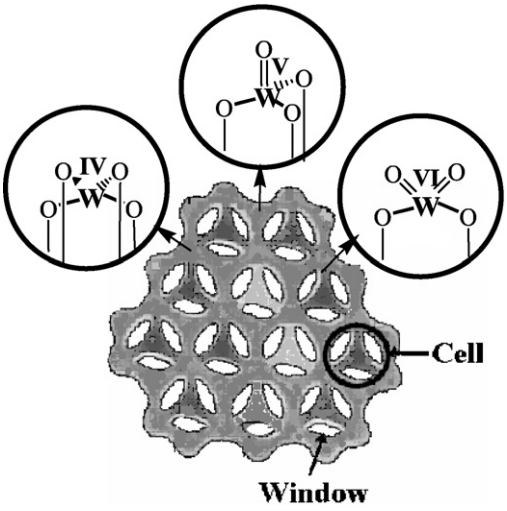

Scheme 2. Incorporating catalytic oxotungsten tetrahedra centers into the framework maintains the structure of MCF.

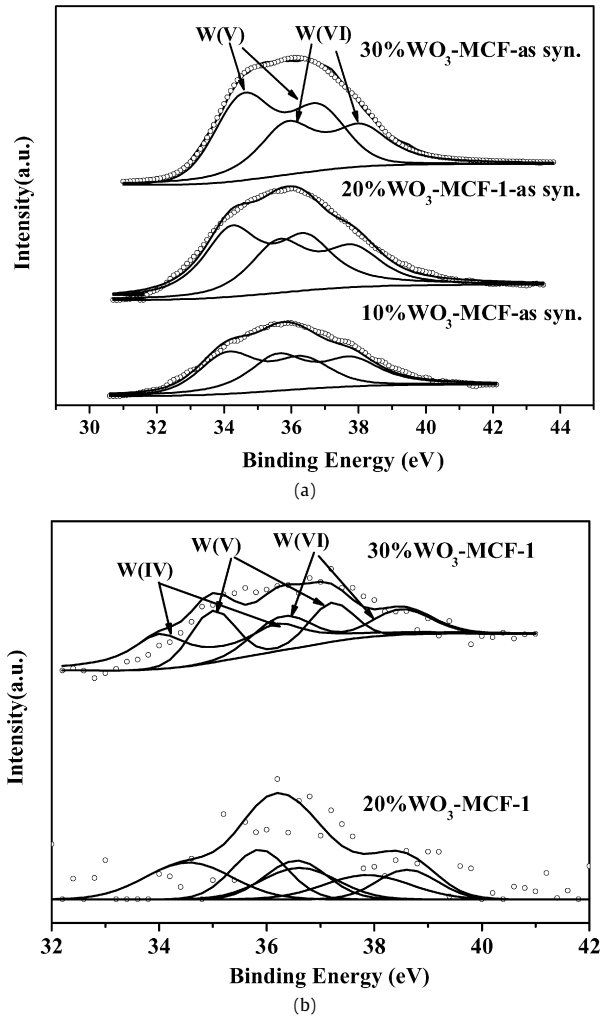

Fig. 6. XPS spectra of the W4f region for the as-synthesized different WO_3 loading catalysts (a) and the AMA-treated different WO_3 loading catalysts (b).

3.1.6. Chemical states by XPS

From the W4f XPS spectra of the WO_3-containing MCF and the AMA-treated samples given in Fig. 6, we can distinguish tungsten oxide species in different chemical states from the position of the W4f level by the curve-fitting procedure. Detailed quantitative results from the peak-fitting results of W4f are given in Table 4. The measured spectra appear to be similar for all of the as-synthesized samples and show identical positions of the W4f peaks, except for the minor charging effect observed and corrected for according to the contaminant carbon (C1s = 284.6 eV). Both W(VI) and W(V) species at W4f7/2 (of 36.6 and 34.6 eV [40,41]) for the W4f spin–orbit components were detected for the as-synthesized samples. It can be seen that the intensity of the W4f XPS peaks also increased with increasing tungsten oxide loading, as illustrated by the changes in relative peak areas for W4f shown in Fig. 5a. Moreover, the intensity of the W4f XPS peaks was much weaker in the AMA-treated samples than in the as-synthesized samples. It is also very interesting that the W(IV) species appeared after AMA treatment, according to the peak-fitting results of W4f, indicating that all of the loosely bound tungsten species were removed, and that the remaining species were the most stable with isolated structures. According to findings of our previous work, single-site tungsten species can be present with an oxidation state of IV or V [42].

Table 4
Peak-fitting results of W4f region for the as-synthesized different WO_3 loading catalysts and the AMA-treated catalysts

Sample	Binding energy for W4f (eV)						
	W^{6+} 4f5/2	W^{6+} 4f7/2	W^{5+} 4f5/2	W^{5+} 4f7/2	W^{4+} 4f5/2	W^{4+} 4f7/2	W^{6+}/W^{5+}[a]
WO_3[b]	38.0	36.0	–	–	–	–	–
$WO_{2.5}$[b]	–	–	36.8	35.0	–	–	–
10%WO_3-MCF-as syn.	38.4	36.6	36.8	35.0	–	–	1.7
20%WO_3-MCF-as syn.	38.4	36.6	36.8	35.0	–	–	1.8
30%WO_3-MCF-as syn.	38.5	36.7	36.8	35.0	–	–	2.0
20%WO_3-MCF-1	38.4	36.6	37.4	35.6	36.3	34.5	1.0
30%WO_3-MCF-1	38.1	36.3	36.9	35.1	35.8	34.0	0.8

[a] Calculated according to the curve-fitting results of the W4f XPS spectra of catalysts.
[b] See reference: Appl. Catal. A 269 (2004) 169–177.

Table 5
Epoxidation of COD over the different catalysts

Catalyst	S_{MD} (%)	TOF[a] (h^{-1})	H_2O_2 utility[b] (%)
10%WO_3-MCF-1	92.7	17.8	43.6
10%WO_3/MCF-1	68.5	4.3	20.2
10%WO_3-SBA-15-1	88.2	10.4	22.9
10%WO_3/SBA-15-1	79.8	2.2	22.1
10%WO_3/MCM-41-1	81.0	0.56	8.2

Reaction conditions: reaction temperature 60 °C, COD: 0.53 mL, H_2O_2: 0.7 mL, reaction time 24 h, *t*-BuOH: 10 mL, cat.: 0.2 g.
[a] Calculated according to the equation: TOF = moles of COD converted per mole of WO_3 per hour.
[b] H_2O_2 utility (%) = $(C_{COD} \times S_{MD})/3C_{H_2O_2}$ (C_{COD}: conversion of H_2O_2; S_{MD}: selectivity of COD epoxide; $C_{H_2O_2}$: conversion of H_2O_2).

As also shown in Table 4, the W^{6+}/W^{5+} molar ratio increased from 1.7 to 2.0 as the WO_3 content rose from 10 to 30%, suggesting a higher content of surface W^{6+} species and much greater formation of crystalline WO_3 species in the 30 wt% WO_3-containing MCF sample. In the AMA-treated samples, however, the W^{6+}/W^{5+} molar ratios dropped to about half of the initial values, demonstrating that the W^{6+} species were located mainly on the surface of the samples and could be removed by AMA treatment. (The XPS spectra of the AMA-treated 10%WO_3-MCF-1 also were detected, but the signal was too weak for ready analysis.) This finding suggests that high polymeric tungsten species were completely removed after AMA treatment.

3.2. Catalytic activity tests in the epoxidation of COD by aqueous H_2O_2

3.2.1. Effect of the different supports

Table 5 presents the results of COD epoxidation over W-containing MCF, SBA-15, and MCM-41. Blank experiments per-

Table 6
Influence of the WO_3 loadings and AMA-treated cycles

Catalyst	S_{MD} (%)	TOF[a] (h^{-1})	H_2O_2 utility[b] (%)
10%WO_3-MCF-1	92.7	17.8	43.6
10%WO_3-MCF-2	91.7	16.6	58.8
20%WO_3-MCF-1	86.4	10.4	53.0
20%WO_3-MCF-2	87.0	15.4	53.4
30%WO_3-MCF-1	59.4	4.0	37.8
30%WO_3-MCF-2	85.0	14.0	28.9
10%WO_3/MCF-1	68.5	3.0	20.2
10%WO_3/MCF-2	94.1	3.6	51.0
10%WO_3/MCF-3	93.2	3.4	50.0

Reaction conditions: reaction temperature 60 °C, COD: 0.53 mL, H_2O_2: 0.7 mL, reaction time 24 h, *t*-BuOH: 10 mL, cat.: 0.2 g.

[a] Calculated according to the equation: TOF = moles of COD converted per mole of WO_3 per hour.

[b] H_2O_2 utility (%) = $(C_{COD} \times S_{MD})/3C_{H_2O_2}$ (C_{COD}: conversion of H_2O_2; S_{MD}: selectivity of COD epoxide; $C_{H_2O_2}$: conversion of H_2O_2).

formed with no catalysts or with purely siliceous supports demonstrated no conversion of COD (results not given). Comparing the findings for 10%WO_3-MCF-1 and 10%WO_3-SBA-15-1 reveals a greater selectivity to COD epoxide and TOF values in the former than in the latter, indicating that MCF's ultra-large pores and unique 3-D cell-window structure lead to better catalytic activity and selectivity. Meanwhile, comparing the findings for 10%WO_3/MCF-1, 10%WO_3/SBA-15-1 and 10%WO_3/MCM-41-1 shows that 10%WO_3/MCF-1 was the most effective catalyst. These findings also demonstrate that MCF's ultra-large pores and the unique 3-D cell-window structure make this more favorable for the title reaction compared with the SBA-15 and MCM-41, which only have 2-D pore structures.

We also investigated the effect of the two preparation methods. The *in situ*-derived 10%WO_3-MCF-1 demonstrated better catalytic performance than the impregnation-derived 10%WO_3/MCF-1. This difference may be attributed to the different states of the tungsten species over these two catalysts. Similar results also were obtained for the 10%WO_3-SBA-15-1 and 10%WO_3/SBA-15-1 catalysts. Table 5 also presents H_2O_2 utility findings. As shown, the H_2O_2 utility was greatest in the 10%WO_3-MCF-1, in line with this catalyst's highest activity.

3.2.2. Effect of WO_3 loading and AMA-treated cycles

Table 6 presents the reaction results as a function of the WO_3 loading and AMA-treated cycles. The TOF value clearly decreased with increasing tungsten loading, as did the selectivity to COD epoxide. The catalytic performance of the three WO_3 loading catalysts differed after one AMA treatment but became similar after two AMA treatments, indicating that the catalytic behavior of the tungsten-containing silica catalysts was affected by the intrinsic nature of tungsten oxide species. The 10%WO_3-MCF-1 and 10%WO_3-MCF-2 demonstrated no change in tungsten loading and the tungsten species. In both catalysts, the dominant tungsten species were the isolated tetrahedral $[WO_4]^{2-}$ species; thus, the two catalysts exhibited similar catalytic performance. The TOF value was higher in the 20%WO_3-MCF-2 than in the 20%WO_3-MCF-1. In the 20%WO_3-MCF-1, the dominant tungsten species were the isolated tetrahedral $[WO_4]^{2-}$ species and low-condensed polymeric tungsten oxide species; however, in the 20%WO_3-MCF-2, the dominant tungsten species were isolated tetrahedral $[WO_4]^{2-}$ species. This indicates that the highly active and selective tungsten species for the title reaction were the isolated tetrahedral $[WO_4]^{2-}$ species. The catalytic performance of the 30%WO_3-MCF-1 and 30%WO_3-MCF-2 also demonstrates that the isolated tetrahedral $[WO_4]^{2-}$ species are the most active and selective tungsten species for the title reaction. Analogously, previous studies have shown that the isolated tetrahedral vanadium oxide species are active for the partial oxidation of methane [16]. Moreover, the 10%WO_3-MCF-2 can be seen to have the highest H_2O_2 utility of all of the catalysts according to the same deductive process.

Table 7
Influence of the calcination temperature on the catalytic performance of 10%WO_3-MCF

Temperature (°C)	S_{MD} (%)	TOF[a] (h^{-1})	H_2O_2 utility[b] (%)
10%WO_3-MCF-syn.-1	89.0	0.2	34.3
10%WO_3-MCF-300-1	90.0	11.3	31.0
10%WO_3-MCF-500-1	92.7	17.8	43.6
10%WO_3-MCF-700-1	95.0	3.9	49.5
10%WO_3-MCF-900-1	96.0	3.9	50.1

Reaction conditions: reaction temperature 60 °C, COD: 0.53 mL, H_2O_2: 0.7 mL, reaction time 24 h, *t*-BuOH: 10 mL, cat.: 0.2 g.

[a] Calculated according to the equation: TOF = moles of COD converted per mole of WO_3 per hour.

[b] H_2O_2 utility (%) = $(C_{COD} \times S_{MD})/3C_{H_2O_2}$ (C_{COD}: conversion of H_2O_2; S_{MD}: selectivity of COD epoxide; $C_{H_2O_2}$: conversion of H_2O_2).

For the AMA-treated 10%WO_3/MCF catalysts, the catalytic performance of the 10%WO_3/MCF-3 was similar to that of the 10%WO_3/MCF-2 and differed from that of the 10%WO_3/MCF-1, indicating that the catalytic behavior of these catalysts was affected by the intrinsic nature of tungsten oxide species. No changes in tungsten loading or tungsten species were seen; the most dominant tungsten species were the isolated tetrahedral $[WO_4]^{2-}$ species and some low-condensed polymeric tungsten oxide species. Consequently, the 10%WO_3/MCF-3 and 10%WO_3/MCF-2 demonstrated similar catalytic performance. Meanwhile, for 10%WO_3/MCF-1, the dominant tungsten species were the isolated tetrahedral $[WO_4]^{2-}$ species and some low-condensed polymeric tungsten oxide species; thus, the catalytic performance of the 10%WO_3/MCF-1 differed from that of 10%WO_3/MCF-3 and 10%WO_3/MCF-2. The *in situ*-prepared 10%WO_3-MCF-2 also had a higher TOF value than the impregnation-prepared 10%WO_3/MCF-3, indicating that the isolated tetrahedral $[WO_4]^{2-}$ species were the most highly active sites, although the low-condensed polymeric tungsten oxide species also showed some activity.

3.2.3. Effect of the calcination temperature

Table 7 characterizes the effect of calcination temperature on the catalytic behavior of the 10%WO_3-MCF catalyst. The catalyst exhibited its best performance to COD epoxide at a calcination temperature of 500 °C. Calcination temperatures above or below 500 °C all led to decreased activity. The TOF values unambiguously verify this conclusion; however, it should be noted that the TOF value was sharply decreased at a calcination temperature of 700 °C. These results can be explained by the gradual decomposition of the intrinsic structure of the active species on the catalyst at calcination temperatures of 700 °C and above. Thus, 500 °C was chosen as the optimum calcination temperature for the 10%WO_3-MCF catalyst, because the tungsten oxide species could not be fully activated at lower calcination temperature. However, the 10%WO_3-MCF calcined at 700 and 900 °C exhibited greater H_2O_2 utility and selectivity than the other catalyst even though they had much lower TOF values, indicating that most of the active tungsten species were destroyed by treatment at elevated temperatures and the ones that remained were the most stable isolated tetrahedral $\{WO_4\}$ species.

3.2.4. Time course of COD oxidation over 10%WO_3-MCF-1 catalyst

Scheme 1 shows the main product, COD epoxide, as well as the main byproducts detected by GC-MS analyses. The finding of no products from the *O*-heterocyclization of COD [27] is surprising, indicating that the isolated tetrahedral $\{WO_4\}$ species played an important role in the epoxidation of cycloocta-1,5-diene. Fig. 7 illustrates the dependence of COD conversion and the selectivity to COD epoxide on the reaction time over the 10%WO_3-MCF-1 cat-

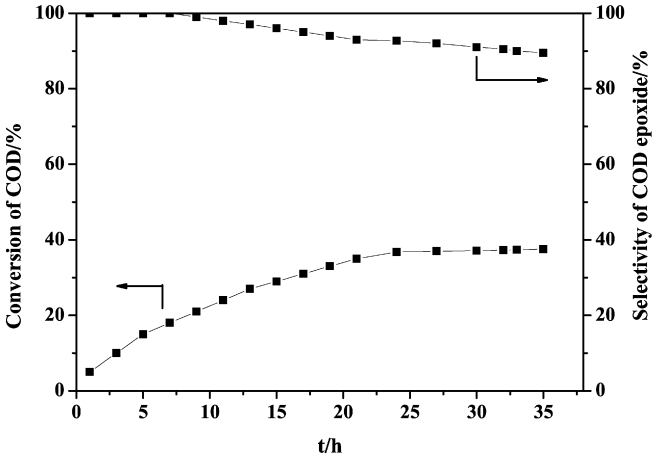

Fig. 7. The dependence of the coversion of COD and the selectivity of COD epoxide on the reaction time over the 10%WO_3-MCF-1 catalyst. Reaction condition: reaction temperature: 60 °C, COD: 0.53 mL, H_2O_2: 0.7 mL, *t*-BuOH: 10 mL, cat.: 0.2 g.

Table 8
Reusability of 10%WO_3-MCF-1

Entry	S_{MD} (%)	TOF[a] (h^{-1})	H_2O_2 utility[b] (%)
1	92.7	17.8	43.6
2	92.0	16.4	54.9
3	87.2	16.9	46.2
4	88.1	16.4	52.8
5	87.0	17.4	43.6

Reaction conditions: reaction temperature 60 °C, COD: 0.53 mL, H_2O_2: 0.7 mL, reaction time 24 h, *t*-BuOH: 10 mL, cat.: 0.2 g.

[a] Calculated according to the equation: TOF = moles of COD converted per mole of WO_3 per hour.

[b] H_2O_2 utility (%) = $(C_{COD} \times S_{MD})/3C_{H_2O_2}$ (C_{COD}: conversion of H_2O_2; S_{MD}: selectivity of COD epoxide; $C_{H_2O_2}$: conversion of H_2O_2).

alyst. The conversion of COD increased with reaction time over the first ~24 h, then remained almost the same with further increases in reaction time. The selectivity of COD epoxide was 100% initially and decreased slowly thereafter. Based on these findings, we propose that COD epoxide is an intermediate from which the byproducts are produced through its further oxidation and further reaction with water.

3.2.5. Reusability of the 10%WO_3-MCF-1 catalyst

To investigate the stability of active tungsten species in the 10%WO_3-MCF-1 catalyst, the leaching of WO_x species into the reaction mixture and the tungsten remaining in the catalyst were also determined by ICP analysis after five reaction cycles. No detectable leaching of W-species or obvious loss of tungsten in the 10%WO_3-MCF-1 catalyst was observed, demonstrating the presence of strong interactions between active tungsten species and the silica-based matrix with the MCF structure. When the reaction over WO_3-MCF catalyst was carried out for 10 h, the catalyst was removed through simple filtration, and the reaction solution was stirred for another 14 h. No detectable increases in the conversion and yield of COD epoxide were found, indicating that the reaction was not influenced by the homogeneous catalysis. Table 8 also gives results of the selective oxidation of COD to epoxide over the 10%WO_3-MCF-1 catalyst with different reaction cycles and the postregeneration material. After the fifth cycle, the selectivity of the object product remained the same, and the TOF values were as high as those for the fresh catalyst. In conclusion, the 10%WO_3-MCF-1 catalyst demonstrated high stability as well as excellent activity for the selective oxidation of COD to COD epoxide. The H_2O_2 utility was close to 50% for both the fresh and recycled 10%WO_3-MCF-1 catalyst.

4. Conclusion

The AMA-treated WO_3-MCF catalysts exhibited good performance, which has been attributed to the ultra-large mesopores of the catalysts for this reaction. The AMA-treated catalysts retained the special structure of the supports under our treatment conditions. The most highly isolated tungsten atoms were well embedded into the supports when the catalysts were treated with AMA, as demonstrated by UV–vis DRS, XPS, and UV-Raman experiments. The UV–vis DRS results also showed that the crystalline tungsten trioxide species were removed first, followed by the polymeric WO_3 species. The tungsten percent maintained a fixed value for the catalysts with different WO_3 loadings, as confirmed by ICP analysis. Different preparation methods led to different final residual tungsten percents, but only the *in situ* method led to the perfect single-site {WO_4} tetrahedral species. The recycling experiment demonstrated the excellent stability of the AMA-treated WO_3-MCF catalyst.

Acknowledgments

This work was supported by the Major State Basic Resource Development Program (Grant 2003CB615807), the NSFC (Projects 20407006 and 20573024), and the Natural Science Foundation of Shanghai Science and Technology Committee (Grant 06JC14004).

References

[1] R.D. Wilson, D.G. Barton, C.D. Baertsch, E. Iglesia, J. Catal. 194 (2000) 175.
[2] B.F. Sels, D.E. De Vos, P.A. Jacobs, Angew. Chem. Int. Ed. 44 (2005) 310.
[3] C.D. Baertsch, K.T. Komala, Y.H. Chua, E. Iglesia, J. Catal. 205 (2002) 44.
[4] T. Kabe, W.H. Qian, A. Funato, Y. Okoshi, A. Ishihara, Phys. Chem. Chem. Phys. 5 (1999) 921.
[5] Y. Rezgui, M. Guemini, Appl. Catal. A 282 (2005) 45.
[6] U. Ciesla, D. Demuth, R. Leon, P. Petroff, G. Stucky, K. Unger, F. Schüth, J. Chem. Soc. Chem. Commun. (1994) 1387.
[7] M.J. Yuan, Z. Shan, B.Z. Tian, B. Tu, P.Y. Yang, D.Y. Zhao, Microporous Mesoporous Mater. 78 (2005) 37.
[8] X.L. Yang, W.L. Dai, C.W. Guo, H. Chen, Y. Cao, H.X. Li, H.Y. He, K.N. Fan, J. Catal. 234 (2005) 438.
[9] C. Martin, P. Malet, G. Solana, V. Rives, J. Phys. Chem. B 102 (1998) 2759.
[10] F. Somma, G. Strukul, J. Catal. 227 (2004) 344.
[11] Z.R. Zhang, J.S. Sue, X.M. Zhang, S.B. Li, Chem. Commun. (1998) 241.
[12] E. Briot, J.Y. Piquemal, M. Vennat, J.M. Brégeault, G. Chottard, J.M. Manoli, J. Mater. Chem. 10 (2000) 953.
[13] W.L. Dai, H. Chen, Y. Cao, H.X. Li, S.H. Xie, K.N. Fan, Chem. Commun. (2003) 892.
[14] X.L. Yang, W.L. Dai, H. Chen, J.H. Xu, Y. Cao, H.X. Li, K.N. Fan, Appl. Catal. A 283 (2005) 1.
[15] J.E. Herrera, J.H. Kwak, J.Z. Hu, Y. Wang, C.H.F. Peden, J. Macht, E. Iglesia, J. Catal. 239 (2006) 200.
[16] H. Berndt, A. Martin, A. Brückner, E. Schreier, D. Müller, H. Kosslick, G.-U. Wolf, B. Lücke, J. Catal. 191 (2000) 384.
[17] P. Rybarczyk, H. Berndt, J. Radnik, M.-M. Pohl, O. Buyevskaya, M. Baerns, A. Brückner, J. Catal. 202 (2001) 45.
[18] M. Santhosh Kumar, M. Schwidder, W. Grünert, A. Brückner, J. Catal. 227 (2004) 384.
[19] J.C. Groen, A. Brückner, E. Berrier, L. Maldonado, J.A. Moulijn, J. Pérez-Ramírez, J. Catal. 243 (2006) 212.
[20] M. Santhosh Kumar, M. Schwidder, W. Grünert, U. Bentrup, A. Brückner, J. Catal. 239 (2006) 173.
[21] M.L. Wang, T.H. Huang, React. Kinet. Catal. Lett. 78 (2003) 275.
[22] E. Larsen, K.A. Jøgensen, Acta Chem. Scand. 43 (1989) 250.
[23] G. Legemaat, W. Drenth, J. Mol. Catal. 62 (1990) 119.
[24] R.U. Pillai, S.E. Demessie, Green Chem. 4 (2002) 495.
[25] E. Brule, R.d.Y. Miguel, K.K. Hii, Tetrahedron 60 (2004) 5913.
[26] R.U. Pillai, S.E. Demessie, S.R. Varma, Tetrahedron Lett. 43 (2002) 2909.
[27] R.H. Gao, W.L. Dai, X.L. Yang, H.X. Li, K.N. Fan, Appl. Catal. A 332 (2007) 138.
[28] C.Y. Cheng, K.J. Lin, M.R. Prasad, S.J. Fu, S.Y. Chang, S.G. Shyu, H.S. Sheu, C.H. Chen, C.H. Chuang, M.T. Lin, Catal. Commun. 8 (2007) 1060.
[29] P. Schmidt-Winkel, W.W. Lukens Jr., P. Yang, D.I. Margolese, J.S. Lettow, J.Y. Ying, G.D. Stucky, Chem. Mater. 12 (2000) 686.
[30] D.Y. Zhao, J.L. Feng, Q.S. Huo, N. Melosh, G.H. Fredrickson, B.F. Chmelka, G.D. Stucky, Science 279 (1998) 548.

[31] D.Y. Zhao, Q.S. Huo, J.L. Feng, B.F. Chmelka, G.D. Stucky, J. Am. Chem. Soc. 120 (1998) 6024.
[32] J.S. Beck, J.C. Vartuli, W.J. Roth, M.E. Leonowicz, C.T. Kresge, K.D. Schmitt, C.T.-W. Chu, D.H. Olson, E.W. Sheppard, S.B. McCullen, J.B. Higgins, J.L. Schlenker, J. Am. Chem. Soc. 114 (1992) 10834.
[33] P. Schmidt-Winkel, W.W. Lukens Jr., D. Zhao, P. Yang, B.F. Chmelka, G.D. Stucky, J. Am. Chem. Soc. 121 (1999) 254.
[34] Y. Wang, Q.H. Zhang, Y. Ohishi, T. Shishido, K. Takehira, Catal. Lett. 72 (2001) 215.
[35] C.W.F.T. Pistorius, J. Chem. Phys. 44 (1966) 4532.
[36] O. Klepel, W. Böhlmann, E.B. Ivanov, V. Riede, H. Papp, Microporous Mesoporous Mater. 76 (2004) 105.
[37] R.S. Weber, J. Catal. 151 (1995) 470.
[38] J.G. Wu, S.B. Li, J. Phys. Chem. 99 (1995) 4566.
[39] K.J. Chao, C.N. Wu, H. Chang, L.J. Lee, S.F. Hu, J. Phys. Chem. B 101 (1997) 6341.
[40] F. Le Normand, J. El Fallah, L. Hilaire, P. Lègarè, A. Kotani, J.C. Parlebas, Solid State Commun. 71 (1989) 885.
[41] M. Valigi, D. Gazzoli, I. Pettiti, G. Mattei, S. Colonna, S. De Rossi, G. Ferraris, Appl. Catal. A 231 (2002) 159.
[42] X.L. Yang, W.L. Dai, R.H. Gao, K.N. Fan, J. Catal. 249 (2007) 278.